Published in final edited form as:
Ind Eng Chem Res. 2012 July 18; 51(28): 9581–9590. doi:10.1021/ie301031u.

Iron-Based Nanoparticles for Toxic Organic Degradation: Silica Platform and Green Synthesis

Noah D. Meeks[**], **Vasile Smuleac**, **Christopher Stevens**, and **Dibakar Bhattacharyya**[*] **[Chair Professor]**
Dept. of Chemical and Materials Engineering University of Kentucky Lexington, KY 40506-0046 USA

Abstract

Iron and iron oxide nanoparticles (NPs) are finding wide applications for the remediation of various toxic chloro-organic compounds (such as trichloroethylene, TCE), via reductive and oxidative processes. In this study, Fe NPs (30-50 nm) are synthesized by reduction from ferric ions immobilized (by ion exchange) on a platform (two types of sulfonated silica particles), in order to prevent the NP agglomeration. Next, the Fe NPs are oxidized and their effectiveness for the oxidative dechlorination of TCE via the heterogeneous decomposition of hydrogen peroxide to OH• on the surface of the iron oxide NPs was demonstrated. For the reductive approach, the use of ascorbic acid as a "green" reducing agent in conjunction with a secondary metal (Pd) inhibits NP oxidation and agglomeration through surface adsorbed species. The Fe/Pd NPs have been successfully applied for the dechlorination of TCE (k_{SA}, surface-area normalized reaction rate, = 8.1×10^{-4} L/m^{2}h).

Keywords

silica; iron; palladium; ascorbic acid; trichloroethylene; dechlorination

1. Introduction

The use of catalytic and reactive nanoparticles in various environmental applications is an emerging field; however, their use has been limited because of several practical difficulties. Among these, the major ones are NP aggregation and surface deactivation (through oxidation or passivation). This is especially true for magnetic and electropositive zero-valent metal NP, such as iron.[1] Various methods for Fe NP synthesis have been described in literature,[2,3] one of the most common being the reduction of inorganic iron salts using sodium borohydride[4] (1).

$$Fe(H_2O)_6^{3+} + 3BH_4^- + 3H_2O \rightarrow Fe^0 + 3B(OH)_3 + 10.5H_2 \quad (1)$$

Naturally occurring reducing agents can be used in the place of borohydride, especially in the synthesis of iron nanoparticles with the co-reduction of a secondary metal. Recently, the use of ascorbic acid (vitamin C) has been proposed[5] for the co-synthesis of iron and palladium, eliminating the need for post-coating step for the formation of bimetallic NP. Our

[*]Corresponding Author: Dibakar Bhattacharyya University Alumni Chair Professor Dept. of Chemical and Materials Engineering University of Kentucky 177 F. Paul Anderson Tower Lexington, KY 40506-0046 PHONE: (859) 257-2794 FAX: (859) 323-1929 db@engr.uky.edu.
[**]Now affiliated at: Southern Company Research and Environmental Affairs 600 North 18th Street Birmingham, AL 35203 ndmeeks@southernco.com

lab has also recently published the use of polyphenol reduced and stabilized iron particles supported on a functionalized membrane.[6]

Because surface chemistry of nanoparticles plays a prominent role in their application, attempts have been made to stabilize the nanoparticles through chelating ligands, which impede particle agglomeration.[7] The decreased agglomerate size and the presence of the adsorbed polyligands may enhance nanoparticle transport, in some important applications such as groundwater remediation.[8] Various ligands such as polysugars (interacts through hydroxyl groups), carboxymethyl cellulose (CMC)[9] (interacts through both hydroxyl and carboxylate groups), polystyrene sulfonate (PSS),[10] and PSS-containing block co-polymers,[11] have been successfully implemented in the stabilization of Fe NP. A variety of strategies for iron oxide NP stabilization have also been recently reviewed.[12] One study[13] demonstrated the use of metal-carbon bonds for stabilization in non-aqueous solvents, where decylbenzene attached to the surface acts as both a phase transfer agent from the aqueous phase (in which particle is synthesized) to the organic phase in which it is used. Another study[14] showed that non-metal homogeneous nanoparticles may be stabilized by a lack of shear forces during particle formation.

While the chelating ligands do impede particle aggregation, Fe NP have also been successfully synthesized on various platforms for ease of application. Support membranes such as PVDF have been coated with poly(acrylic acid), and this functionalized membrane has been used to immobilize iron ions which are reduced to iron nanoparticles.[15] Activated carbon has been used to support Fe/Pd NPs for the destruction of chloroorganics in aqueous[16] as well as dense non-aqueous phase liquid (DNAPL).[17] Recently published work also describes the synthesis of Pd nanotubes using membrane-based techniques for the destruction of polychlorinated biphenyls PCBs.[18]

The silica platform offers potential advantages over polymers or activated carbon, and it is a well-known support for catalysts. Recently, an ordered mesoporous silica (SBA-15) was optimized for the synthesis of Bi[19] and Co[20] NP by incorporation of precursor salt within the pores. Also Pt NP were formed by the reduction of a precursor salt onto colloidal silica,[21] and both Au[22] and Ti[23] NP have been co-precipitated into sol-gel silica. Some very elegant work[24] has recently been published demonstrating the synthesis of hydrophobized silica particles loaded with Fe NP. In this case, the hydrophobized silica particles are synthesized by direct co-condensation of silane precursors (and simultaneous evaporation of iron salts) in an aerosol-assisted heating process, with the iron salts subsequently reduced to Fe NP using borohydride. A subsequent study indicated the enhanced transport of these materials through simulated aquifers due to decreased aggregation.[25]

In addition to co-condensation of silanes, the silica surface is covered in silanol (SiOH) moieties (typically ~ 3 SiOH/nm^2) which can be easily functionalized using well-known silylation chemistry (2). This is another advantage of silica over other platforms. There are good reviews[26] of silane chemistry and silica functionalization, as well as recent papers from our lab on the extent of functionalization[27] and use of tetrasulfur functionalized particles for mercury vapor sorption.[28] In this case, the silica is functionalized with sulfonate groups which provide a strong ion exchange platform for ferric/ferrous ions. Alternatively a weak ion exchanger such as carboxylate could be used with the ferrous ions only. Although not addressed in this study, multiple functional groups could also be used for the synthesis of hydrophobic/hydrophilic nanodomains. The ability to incorporate multiple functional groups onto a single platform is a further advantage of silica.

$$\mathrm{Si_sOH + X_3SiR \rightarrow Si_sOSi(X)_2R + HX} \quad (\mathrm{X = Cl^-} \text{ or } \mathrm{RO^-} \text{ leaving group}) \quad (2)$$

An important application of zero-valent iron is for the detoxification of trichloroethene (TCE), a very prevalent groundwater pollutant which is both persistent and toxic. Physical as well as chemical oxidation and reduction have been demonstrated for detoxification of TCE. A common physical strategy is air stripping,[29] which may or may not be followed by TCE sorption onto activated carbon. Oxidative strategies include biological oxidation, photocatalytic oxidation,[30] or in situ chemical oxidation (ISCO) techniques, such as Fenton's reaction to generate hydroxyl radicals (OH•).[31] Our lab recently demonstrated the use of modified Fenton's reaction for ISCO; using citrate as a chelating agent for the ferrous/ferric ions to overcome difficulties of conventional Fenton's reaction.[32]

Reduction of TCE can occur by either direct electron transfer or by hydrogenation,[33] and both reactions have been carried out using various catalytic schemes. Although direct electrical current has been shown[34] effective towards TCE reduction, iron is commonly used as an electron-transfer catalyst. Hydrogenation has been carried out by traditional hydrogenation catalysts such as Pd, Ni, Pt, etc., where the hydrogen is supplied. Because the supply of hydrogen to contaminated underground field sites is generally considered impractical, bimetallic catalysts have recently been developed, where a primary metal such as Fe reduces water to hydrogen through corrosion, thus supplying the needed reactant for a nearby hydrogenation catalyst located on the particle surface. Fe/Pd and Fe/Ni[35] bimetallic particles have been shown to be most efficient among various bimetallic combinations.[36] The high surface area to volume ratio of nanoparticles, and the high prevalence of edge defects on nanoscale particles, has been demonstrated to be more effective catalysts than microparticle catalysts.[37]

The objective of this research is to synthesize iron nanoparticles on a sulfonatefunctionalized silica particle platform. The second objective is to further explore iron NP synthesis using “green” reducing agents which can prevent aggregation and also adsorb to the surface and prevent further oxidation. The third objective is to the show reactivity toward environmentally-important compounds such as TCE, using both oxidative and reductive approaches. With each of these objectives, materials synthesis, characterization, application, and discussion will be considered.

2. Experimental Methods

Colloidal silica Ludox TM-50 was obtained from Grace Davison (Columbia, MD) & silica gel from Huber Corp (Havre de Grace, MD). Sulfonated silane reagent, 3-(trihydroxysilyl)-1-propane sulfonic acid (30-35 % in water) (THSPS), was obtained from Gelest Inc. (Morrisville, PA). Palladium tetrachloropalladate were obtained from Sigma-Aldrich. Deionized ultrafiltered (DIUF) water & ethanol were obtained from Fischer Scientific.

2.1 Functionalized Silica Synthesis

Silica particles of various structural dimensions (Table 1) were functionalized with 3-trihydroxylsilyl-1-propane sulfonic acid (THSPS) using previously reported[27] methods without the use of solvents. Briefly, a 3 wt% aqueous solution of THSPS was adjusted to pH = 4.9. Silica particles (10 g in each batch) were dispersed into 50 mL DIUF water and the silane solution (about 75 mL) was injected with vigorous stirring. The mixture was stirred for 15 min to disperse the silane, followed by heating (with stirring) to 100 °C until all water was evaporated. The functionalized particles were cured for 4 h at 100 °C to complete the silylation. They were washed with water to removed excess silane, centrifuged, and dried.

2.2 Extent of functionalization

The extent of functionalization was determined by infrared spectroscopy and thermogravimetric analysis methods given in detail elsewhere.[27] Briefly, a small amount of functionalized particles were finely ground with potassium bromide and pressed into a die. The Fourier transform infrared spectrum was recorded based on 128 scans from 4000 to 400 cm^{-1}. The same procedure was carried out for unfunctionalized particles, and the heights of the Si-O-H peaks at about 980 cm^{-1} were compared; assuming that the loss of silanol groups due to functionalization is proportional to the decrease in Si-O-H peak height. Determining extent of functionalization by thermogravimetric analysis was done by recording the mass loss of a sample as temperature is increased from room temperature to 1000 °C (at a rate of 10 °C/min) in an atmosphere of air. The total mass losses of a functionalized and unfunctionalized sample were compared.

2.3 Silica-Based Fe Particle Synthesis

The first step to forming Fe/Pd particles is to immobilize the ions. The sulfonatefunctionalized silica particles were shaken in a 0.017 *M* ferric chloride ($FeCl_3$•$6H_2O$; 951 mg Fe/L) solution for 12 h. The pH of ferric solution was 2.5 and was unchanged after shaking with the particles, since they were in the Na^+ form (by previously adjusting silane solution pH using NaOH). After centrifugation to remove the particles, the amount of sorbed Fe was determined by measuring the Fe concentration in the supernatant with inductively coupled plasma (ICP) at multiple wavelengths. Next, the immobilized ferric ion was reduced to zero-valent iron (ZVI) by borohydride. A freshly prepared 0.17 *M* solution (50 mL) $NaBH_4$ was added dropwise to a beaker containing about 20 mg of Fe immobilized on ~3 g silica dispersed in 100 mL deoxygenated water. The particles turned gray due to the formation of black iron particles on the white silica surface. The reduction was allowed to continue for 1 h, and the silica/Fe particles were centrifuged, washed with ethanol, and dried. In the case of particles silica-based particles used for oxidative dechlorination reactions, the Fe NP were oxidized using air bubbled through a dispersion of these particles in water for up to 24 h. The iron oxide/iron particles on silica were then centrifuged and dried.

2.4 Ascorbic acid as a reducing agent

Besides immobilization or the use of polyligands, another method to synthesize particles while inhibiting oxidation and aggregation is to use natural weak reducing agents, such as ascorbic acid. Excess reducing agent adsorbs to the particle surface to prevent oxidation of the particle, and various surface adsorbed species can also inhibit aggregation. Ascorbic acid is a weak reducing agent, and therefore will not sufficiently reduce iron without the presence of another reduction reaction. Therefore, bimetallic Fe/Pd particles were prepared by the co-reduction of $FeCl_3$•$6H_2O$ and K_2PdCl_4 with ascorbic acid, which is a modification of a recent procedure.[5] Briefly, for each batch prepared, 10 mL of a 0.1 M ascorbic acid solution was mixed with 20 mL of 0.01 M ferric solution ($FeCl_3$•$6H_2O$). Particles were formed upon the addition of $PdCl_4^{2-}$ solution (10:1 Fe:Pd ratio). Alternatively, Pd can be prepared alone by reduction with ascorbic acid: particles were first prepared by reducing $PdCl_4^{2-}$ to Pd^0 using ascorbic acid in ten times the stoichiometric amount, 23.1 mM ascorbic acid solution was used with four times the volume of Pd(II) solution. Upon reaction, the solution turned immediately gray. Then, Pd particles were prepared in various ascorbic:Pd molar ratios for analysis.

2.5 Metal particle characterization

Metal or bimetallic particles were characterized using several methods. Nitrogen sorption data at 77K was obtained using a Micromeritics Tristar 3000 instrument. Surface adsorbed

species were detected by Nicolet Nexus 470 infrared spectrometer running Omnic software. Particle morphology was determined in Jeol 2100 TEM at 200kV accelerating potential on a copper grid. Dynamic light scattering (Beckman Coulter Delsa Nano C Particle Analyzer) was used to determine hydrodynamic radius.

2.6 TCE degradation experiments

TCE degradation experiments were carried out in 20 mL EPA glass vials with a gas-tight PTFE-coated PDMS septum. Samples were initially loaded with particles and TCE solution (20-30 mg/L). A control vial was prepared without particles to ensure that no TCE was volatilized. The concentration of TCE in a sample was determined after a certain time interval by extraction of the sample with pentane (5 μL ethylene dibromide (EDB) as an internal standard, per 100 mL pentane) and analysis using gas chromatography (HP Series II model 5890) with a mass spectrometer (HP 5971A) detection system (GC-MS). Each sample was used for only a single data point. Standard solutions (1 to 30 mg/L) of TCE in pentane were prepared, also using EDB as an internal standard. The lowest detection limit was 1 mg/L TCE in pentane.

For oxidative dechlorination experiments (using oxidized particles), each sample vial was loaded with reactive particles (average loading = 0.16 g/L Fe; detected by acid digestion followed by atomic absorption), hydrogen peroxide ($C_{initial}$ = 1409 mg/L), and TCE ($C_{initial}$ = 22 mg/L) in deoxygenated water. Each vial (20 mL clear EPA vial with Teflon-coated septum) was shaken for a time and opened only once, where 4 mL of the solution was removed. This solution was extracted by shaking with the EDB-containing pentane. After 2 h extraction, the concentration of TCE in the pentane was determined by GC-MS. For reductive dechlorination experiments, the same sampling and analysis procedure was used. The initial concentrations were 1 g/L Fe loading, 30 mg/L TCE, and no hydrogen peroxide.

3. Results and Discussions

The two schemes presented in Figure 1 were used to synthesize silica-based iron and iron/iron oxide nanoparticles, and ascorbic acid-stabilized Fe/Pd bimetallic nanoparticles. The first objective of this research was to quantify the silica functionalization, to characterize the Fe NP and the oxidized Fe NP (for dechlorination), and to demonstrate the utility for dechlorination. The second objective was to synthesize, characterize, and demonstrate the reductive dechlorination of the ascorbic acid-stabilized Fe/Pd bimetallic particles. These are also compared and contrasted with results from similar recent studies to show key outcomes.

3.1 Unfunctionalized Silica Characterization

Two types of silica were functionalized with 3-(trihydroxysilyl)-1-propanesulfonic acid (“THSPS”). One type of silica used is Ludox TM-50 colloidal silica from Grace Corp. The manufacturer reported these to be monodisperse 22 nm silica spheres, and SEM measurements as well as dynamic light scattering measurements previously performed in our lab have confirmed this. This type of colloidal silica has no intraparticle pore structure, only gaps between particles. The surface area (A_S) of 22 nm solid silica spheres, assuming no aggregation, is computed geometrically (using density, ρ, of 2.65 g/cm^3) to be 103 m^2/g, using (3).

$$A_S = \frac{4\pi r^2}{\frac{4}{3}\pi r^3 \rho} = \frac{3}{r\rho} \quad (3)$$

However due to aggregation during the required drying to nitrogen sorption measurements, the BET surface area was computed to be 87 m^2/g. The other type of silica used is porous

silica gel, with 3 μm particles, and a wide distribution of intraparticle pores (average diameter ~10 nm) has a BET surface area of 585 m^2/g.

3.2 Extent of Silica Functionalization

The extent of functionalization is determined through two methods, IR spectroscopy and TG analysis. Using the IR spectra, the relative heights of the SiOH vibration (980 cm^{-1}) are compared. Although another OH vibrations is present (the broad peak around 3400 cm^{-1}), this is not suitable for analysis as it decreases with the removal of surface bound water as well as the condensation of silanol groups with the silane. For the Ludox, IR spectra (Figure 2a) indicate that 47 % of the silanol groups are reacted after sulfonate functionalization. For the silica gel, IR spectra indicate that 68 % surface silanol groups are reacted. These are consistent with previous functionalization results for these silica platforms in our lab.[27] Extent of silica functionalization (g silane / g silica or % silane) is computed from TGA (Figure 2b) data. Using the high temperature data of mass loss, the extent of silica functionalization is given by

$$\%\ \text{silane} = \text{mass at}\ \ 120\ \ ^{\circ}\text{C}\ \ -\ \ \text{mass at}\ \ 800\ \ ^{\circ}\text{C} \quad (4)$$

TGA indicates that the organic silane is 10 mass% of the functionalized Ludox particles. For the functionalized silica gel, organic silane is 7.0 mass%. Using the nitrogen sorption data, the sulfonate (silane) groups per nm^2 (α_{SO3}) is approximated, and the original silanol number (α_{SiOH}), before the functionalization, can also be theoretically calculated.

$$\alpha_{SO3} = \frac{sulfonate}{nm^2} = \frac{\%\ \ silane \times N_A}{A_S \times MW_{silane} \times 100 \times 10^{18}} \quad (5)$$

MW_{silane} is the molar mass of organic portion of the silane, as the new siloxane bond should be stable against thermal degradation; the value used is 158.2 (calculated by subtracting MW for one Si and one Oxygen from MW of the silane). N_A is Avogadro's number, and A_S is surface area of functionalized silica in m^2/g. Using these theoretical calculations, for functionalized Ludox, α_{SO3} = 4.1 and for functionalized silica gel, α_{SO3} = 0.95. The computed cross-sectional area of THSPS is 0.2855 nm^2 (using Chemicalize beta software, http://www.chemicalize.org). For silica gel, the α_{SO3} = 0.95 is very reasonable, as two THSPS molecules would occupy a cross sectional area of 0.27 nm^2. However, for Ludox, the theoretically calculated α_{SO3} = 4.1 is too large to occupy the silica surface, indicating the presence of multilayer silane network around the Ludox silica nanoparticles. Based on the number of number of silanol groups reacted (from IR data), and the TG data, it is possible to compute the original silanol number (α_{SiOH}).

$$\alpha_{SiOH} = \frac{silanol}{nm^2} = \frac{100 \times \alpha_{SO3}}{\%\, silanol\ \ \ reacted} \quad (6)$$

For Ludox, α_{SiOH} = 8.9, and for silica gel, α_{SiOH} = 1.4. The highest reported theoretical silanol number is 8,[38] again indicating that for functionalized Ludox, the silane is present as a multilayer network around the silica. For the silica gel, the silanol number is lower than previous reports that have found α_{SiOH} values of 2.9 up to 3.6,[39] indicating that the %silanol calculated by IR has some error.

3.3 Morphology of Functionalized Silica

Functionalization of Ludox doesn't significantly change the BET surface area (87 and 92 m^2/g), because the particles are non-porous. The nitrogen sorption isotherm (Figure S1a) indicates the similar morphology before and after functionalization. The silica gel has a wide

size range of intraparticle pores, and functionalization narrows the pores of all sizes, as well as blocks many of the micropores (Figure S1b). The functionalization of silica gel decreases the BET surface area from 558 m^2/g to 264 m^2/g due to shrinkage and blockage of the pores.

3.4 Iron Immobilization on Functionalized Silica

The first step in synthesis of sulfonated-silica based iron nanoparticles is immobilization of the ferric ions. Both silica platforms indicate the same capacity of Fe^{3+}, about 7.0 mg Fe/g, or 0.125 mmol Fe/g. The immobilization of ferric ions is the same process as conventional sulfonated ion exchange resins. Dow's (Rohm & Haas) Amberlite has total capacity of 0.8 mmol ferric ion/g. However, functionalized silica gel has advantages of open mesoporous structure and also the further advantage of facile multifunctional silylation. The functionalized silica gel (2.0 sulfonate/nm^2) has 2.5 mmol sulfonate/g, indicating an experimental Fe:sulfonate ratio of 0.05. The theoretical Fe:sulfonate ratio is 0.33, indicating that only about 15% of the sulfonate groups are ion-exchanged with Fe^{3+}. For Ludox, the experimental Fe:sulfonate ratio is 0.035, or only 11% of sulfonate groups.

This process exchanges one Fe^{3+} ion for three Na^+ ions (subscript “s” means surface-bound).

$$Fe^{3+} + 3\ Na_s^{+} <=> Fe_s^{3+} + 3\ Na^{+} \quad (7)$$

According to the law of mass action, which describes general exchange equilibria in ionized systems (for surface activity coefficients which are unity), the apparent equilibrium constant, $K^c_{Fe,\,Na}$, is given by

$$K^c_{Fe,Na} = \left(\frac{n_{Fe}}{c_{Fe}}\right)^{z_{Na}} \left(\frac{c_{Na}}{n_{Na}}\right)^{z_{Fe}} \quad (8)$$

where c_i is the supernatant concentration [mol m^{-3}] and n_i is the exchanger-bound concentration [mol kg^{-1} exchanger]. Based on the observed Fe^{3+} supernatant and exchanger-bound concentrations, the equilibrium constant for these functionalized silica platforms as 3.4×10^{-4} (g silica/L)^2.

3.5 Iron Particles on silica

Once ferric ions are immobilized on the sulfonate-functionalized silica, they are reduced to zero-valent iron particles using freshly prepared aqueous sodium borohydride. As it dissolves, the BH_4^- anion reduces water to hydrogen as well as reducing Fe^{3+} to Fe^0; borohydride itself is oxidized to various borate species. The formation of Fe^0 is physically seen as the silica suspension changes from white (silica with ions) to gray (silica with black Fe^0 particles. The agglomeration of the Fe NP (due to both electrostatic and magnetic forces) is limited by the immobilization of the iron on the silica surface and in the pores of the silica gel. The Fe NP with Ludox forms in the sulfonated silane network, resulting in Fe NP that are physically mixed with the colloidal Ludox silica NP.

Transmission electron microscopy (Figure 3) indicates that the iron nanoparticles are located both on the surface and pore mouths of the silica gel, as well as aggregated (apart from the silica surface) in chains that are typical of Fe^0 nanoparticles. Due to the sonication and drying during sample preparation, it is impossible to obtain a true image of the iron nanoparticles during the reactions. However, the particle size of ~50 nm can be determined and elemental analysis (energy dispersive x-ray spectroscopy, EDS) is used to show that they are indeed Fe^0 nanoparticles with a thin oxidized shell due to drying. EDS information alone does not indicate valence state, but the line-scan is used to show that the oxygen

increases near the particle edges, when a thin layer of iron oxide would be the only material present. As the line scan proceeds across the particle, the oxygen content remains constant (from this oxide shell surrounding the particle of constant thickness) even as the iron signal increases due to the increasing depth of the iron core. The particles on the Ludox silica (Figure 4) also were found to be somewhat smaller (~30 nm). The silica nanoparticles are also on the order of that size (22 nm), they form a mixture of silica and agglomerated Fe nanoparticles. EDS line scan indicates that the particle composition is Fe (with Si also indicated because of the proximity to silica particles).

The iron nanoparticle alters the pore structure and surface characteristics of the functionalized material. Fe NP on Ludox (Figure S1b), both microporous and macroporous surface areas increase, corresponding to sorption of nitrogen in the interparticle spacing as well as on the surface of the NP. Overall, the surface area increase for Fe particles on Ludox is from 87 to 110 m^2/g. Using Equation (3), the expected increase in surface area for 30 nm Fe NP would be 25 m^2/g Fe, which is consistent with the experimentally determined increase (23 m^2/g). For the Fe NP on silica gel (Figure S1a), microporous surface area decreases, corresponding to pore blockage. The macroporous surface area increases, corresponding to sorption of nitrogen on surface of the NP. Overall, the BET surface area decreases from 264 to 224 m^2/g.

Silica-based Fe NP have been used as catalysts for well known Fischer-Tropsch hydrocarbon synthesis (particularly when using coal-derived syn gas[40]) and more recently as catalysts for carbon nanotube synthesis.[41] The uniqueness of our system over many previous studies is that functionalized silica was used to immobilize the Fe NP, rather than reduction of Fe salts on the surface or mixed with unfunctionalized silica. Catalytic advantages of silica-supported Fe NP are improved thermal stability, decreased deactivation, and improved selectivity.[42] The silica is thought to play a role in the reduction and drying process which preserves a high surface area. However, Fe NP on silica have been found to have lower activity than those on other supports or unsupported catalysts, due to the stronger interactions between silica and Fe NP including the formation of iron silicate interfacial species.[43] This effect increases with increasing silica:Fe ratio.[42a] Fe NP on silica in these studies have been reported to be 5 to 20 nm.

3.6 Synthesis of Pd and Fe/Pd NP by ascorbic acid

The use of natural products as reducing agents (antioxidants) for the synthesis of metal NP has emerged as an important area of research. Not only are the natural products completely “green” but they also can stabilize the particles against agglomeration and oxidation. Various natural products have been suggested, including the use of polyphenols,[44] commonly found in tea, coffee, wine, and fruit juices. Typically, the E^0 value of these compounds is sufficient to reduce ferrous or even ferric iron to zero-valent iron. Another natural product which has been used is ascorbic acid; however, the reduction potential of ascorbic acid to dehydroascorbic acid is not sufficient to reduce iron alone.[45] The use of ascorbic acid requires a secondary metal, such as Pd, which is reduced along with Fe to form Fe/Pd particles. Although other secondary metals have been described, Pd was chosen because Fe/Pd bimetallic nanoparticles have been shown effective in dechlorination of TCE. The reactions for the formation of Fe/Pd particles are shown in Table 2.

The use of natural reducing agents such as ascorbic acid can stabilize the nanoparticles against oxidation as well as inhibit particle growth. After synthesizing Fe/Pd nanoparticles, an IR spectrum (Figure 5) of the particles was compared to spectra from the pure dehydroascorbic acid and ascorbic acid (chemical structures shown in Figure 1b). The difference between the two compounds is seen by the peak intensity at 1753 cm^{-1} (C=O) and 1660 cm^{-1} (C=C). The shift of the C=C peak in the dehydroascorbic acid is caused by

additional ring strain of three carbonyl moieties on a 5-membered ring. The spectra indicate that both C=O and C=C functional groups were present on the surface, which demonstrates that ascorbate (as pH > 4.17) was adsorbed on the surface, and the peaks have slightly shifted to a lower wavenumber (lower energy). Also, the intensities of the two peaks for the Fe/Pd particles are about the same; for only ascorbic acid, the C=C peak is much more intense than the C=O peak. This may indicate that dehydroascorbic acid (with its more intense C=O peak) is also present on the surface.

The particle size can be limited by use of excess ascorbic acid as indicated by Figure 6. In this case the particles were not Fe/Pd but pure Pd, which has also been used for reductive dechlorination in the presence of supplied hydrogen. The ascorbate adsorbs to the surface and impart a surface charge which inhibits agglomeration. As a higher ascorbic acid:Pd mole ratio was used, the measured hydrodynamic particle radius was significantly lowered, though ascorbic acid:Pd molar ratio >7 rendered no more decrease in size. For this reaction, stoichiometric ratio is 2. Smaller Pd particles have been synthesized by other methods, such as the use of polyligand stabilizers and ascorbic acid reduction,[45] as well as the in vivo synthesis of bio-Pd.[46] However, this simple method yields stable, small Pd or Fe/Pd NP. TEM of the ascorbic acid-synthesized particles at lower pH indicates the unusual growth of crystals with agglomerate diameter ~100 nm (Figure 7). Although the exact role of dehydroascorbic acid and ascorbate in directing the crystal growth is not known, other studies have indicated the synthesis of crystallites of various shapes using natural product reducing agents.[50]

3.7 Oxidative Dechlorination

Recent results have shown success using silica-supported Fe NP for reductive dechlorination of TCE[24]; however, heterogeneous oxidative dechlorination by Fe/Fe_2O_3 particles is an emerging area of research and holds great promise because of the naturally occurring oxidized iron in aquifers and other typically contaminated sites. Oxidative detoxification of TCE is accomplished using Fe/Fe_2O_3 particles as catalysts for the heterogeneous decomposition of H_2O_2, resulting in the formation of OH· (a strong oxidant with $E^0 = 2.73$ V). To show the usefulness of this approach with our silica-based particles, we deliberately oxidized the Fe particles supported on Ludox and tested their efficiency. The primary species present is Fe_2O_3 which may surround a zero-valent Fe core.

The modified Haber-Weiss mechanism is commonly used to describe the decomposition of H_2O_2 on iron oxide surfaces.[48] Although many reactions are involved, the formation of OH· is driven by oxidation (9) of surface ferrous species (≡Fe(II)) and direct decomposition (10) of H_2O_2 by hydroperoxyl radicals (HO_2·). Overall, the decomposition of H_2O_2 is modeled as a heterogeneous pseudo-first order reaction (11).

$$\equiv \mathrm{Fe(II)} + H_2O_2 \rightarrow \equiv \mathrm{Fe(III)} + OH^- + OH\cdot \quad (9)$$

$$H_2O_2 + HO_2\cdot \rightarrow H_2O + O_2 + OH\cdot \quad (10)$$

$$-\frac{dC_{H_2O_2}}{dt} = k_{SA} A_s \rho_m C_{H_2O_2} \quad (11)$$

In the case of our reactions, the Fe loading (0.16 Fe/L) was lower compared to other studies, which slowed the reaction, with initial H_2O_2 concentration of 41.4 mM (1409 mg/L).

The TCE is then oxidized by the generated OH·, which is given as a second order reaction.

$$-\frac{dC_{TCE}}{dt}=kC_{TCE}C_{OH\cdot} \quad (12)$$

Previous studies have found $C_{OH\cdot}$ is small and constant,[49] so that in many cases the oxidation of TCE can be given as pseudo-first order. Pseudo-first-order kinetics have been seen for the Fe-catalyzed oxidation of quinoline[50] (using Fe-containing aquifer material) and trichlorobenzene[51] (using hematite, Fe_2O_3) under reaction conditions similar to this study. However, others have found this Fe-catalyzed oxidation to be pseudo-zeroth order. In this case the decomposition of H_2O_2 was not measured, only the oxidation of TCE. Figure 8 shows the 50% dechlorination in 50 hours of using these particles. However, the result depends on Fe loading and H_2O_2 concentration, as well as Fe:H_2O_2 ratio. The TCE oxidation kinetics fit a first-order reaction with R^2= 0.95 (as shown in Figure 8). The usefulness of Fe/Fe_2O_3-catalyzed production of OH· for oxidative dechlorination is demonstrated. Chloride measurements indicated that after the reaction had ceased (50 hrs), the recovery of Cl^- was 91% of the theoretical Cl^- production, based on 3 mol chloride:1 mole TCE degraded. Given that the initial hydrogen peroxide concentration is high and that its decomposition is proportional to surface area (11), we speculate that the cessation is due to passivation of the Fe surface.

The role of silica in the oxidative dechlorination of TCE is not well understood. Recent reports have speculated that the silica alters the rate of H_2O_2 decomposition because the lower point of zero charge renders the silica-Fe/Fe_2O_3 negatively charged at near neutral pH.[52] Altered rates of decomposition were found to be dependent upon sand species present when using real sand-based Fe oxide catalysts,[50] though efforts to model the complete process were incomplete. It may also be that the surface of the sulfonated silica (Lewis base) impedes the conversion of Fe^{2+} to Fe^{3+}, which is postulated[32] to be the rate-limiting step of the catalytic cycle for H_2O_2 decomposition. However, more study in this area is needed, as recent reports suggest faster and complete decomposition using silica-based iron oxide catalysts, and also incomplete oxidation using soil-based Fe catalysts.

The silica-based iron particles may also be used for reductive degradation of TCE. Recent work[24] shows that unfunctionalized silica containing iron nanoparticles dechlorinated TCE. In the case of partially hydrophobized silica, there was an immediate decrease in the bulk concentration of TCE due to absorption (partitioning of TCE to the hydrophobized surface) followed by quantitative conversion to product after 96 hours reaction. This study also reports the same immediate decrease in bulk TCE concentration, but without destruction, when hydrophobized silica is used without iron.

3.8 Reductive Dechlorination

The overall reductive dechlorination is modeled as a pseudo-first order heterogeneous reaction, and the reaction constant determined by (13).

$$-\frac{dC_{TCE}}{dt}=k_{obs}C_{TCE}=k_{SA}A_s\rho_m C_{TCE} \quad (13)$$

where A_s is specific surface area and ρ_m is the loading of particles. In the case of very small particles (such as those ascorbic acid synthesized particles at near-neutral pH), the specific surface area (A_s) is calculated as surface-to-volume ratio (Equation 3) divided by the intrinsic density of the material (ρ_{Fe} = 7.9 g/cm^3 and ρ_{Pd} = 12.0 g/cm^3). Based on weighted average of Fe/Pd composition (3.8 wt% Pd), the density (ρ) of the Fe/Pd NP is 8.1 g/cm^3. A_s for the ascorbic acid-synthesized Fe/Pd NP (r = 5 nm) are 74.1 m^2/g. Under the reaction conditions described in Figure 9, the k_{SA} is calculated to be 8.1 ×10^{-4} L/m^2h. A recent study

using CMC-stabilized Fe/Pd bimetallic particles indicated k_{SA} of 64 $\times 10^{-4}$ L/m^{2}h for particles with diameter of 4.3 nm.[36] Although the reaction rate is lower than some reported values, these small stable particles may be more useful for reductive dechlorination in dilute TCE-contaminated groundwater plumes, where stability and dispersion of particles is an important consideration.

4. Conclusions

In this study we have demonstrated the stabilization of Fe and Fe/Pd bimetallic NP through use of covalently functionalized sulfonated silica platforms as well as the substitution of borohydride with non-toxic, natural product ascorbic acid as a reducing agent. The silica has a number of advantages including the dispersion of particles to prevent agglomeration and the versatility of surface functionalization. Nanoparticles were effectively synthesized either in the pore mouths or on the surface of silica with different morphologies (colloidal and porous silica gel). The synthesis of stable Fe/Pd NP was also achieved through the use of ascorbic acid as a reducing agent, where the ascorbate (and possibly dehydroascorbic acid) inhibit agglomeration and the excess ascorbic acid protects the surface from oxidation. Both strategies yielded nanoparticles which were reactive toward the detoxification of trichloroethylene, a widespread persistent and toxic water pollutant. One can easily extend our approach to include the synthesis of other moieties on silica platforms to potentially increase partitioning of TCE from water, and also further development of the NP synthesis techniques using other non-toxic natural product reducing agents.

Supplementary Material

Refer to Web version on PubMed Central for supplementary material.

Acknowledgments

The authors acknowledge the NIEHS-SRP program for support of this study. Also, the authors appreciate the contributions of Electron Microscopy Center and Environmental Research Training Laboratory, both at the University of Kentucky. Christopher Stevens was also supported by the NSF/REU program.

References

1. Lu AH, Salabas EL, Schuth F. Magnetic nanoparticles: Synthesis, protection, functionalization, and application. Angew Chem Int Edit. 2007; 46(8):1222–1244.
2. Huber DL. Synthesis, properties, and applications of iron nanoparticles. Small. 2005; 1(5):482–501. [PubMed: 17193474]
3. Tratnyek PG, Nurmi JT, Sarathy V, Baer DR, Amonette JE, Pecher K, Wang CM, Linehan JC, Matson DW, Penn RL, Driessen MD. Characterization and properties of metallic iron nanoparticles: Spectroscopy, electrochemistry, and kinetics. Environ Sci Technol. 2005; 39(5):1221–1230. [PubMed: 15787360]
4. Wang CB, Zhang WX. Synthesizing nanoscale iron particles for rapid and complete dechlorination of TCE and PCBs. Environ Sci Technol. 1997; 31(7):2154–2156.
5. Nadagouda MN, Varma RS. A greener synthesis of core (Fe, Cu)-shell (An, Pt, Pd, and Ag) nanocrystals using aqueous vitamin C. Cryst Growth Des. 2007; 7(12):2582–2587.
6. Smuleac V, Varma R, Sikdar S, Bhattacharyya D. Green synthesis of Fe and Fe/Pd bimetallic nanoparticles in membranes for reductive degradation of chlorinated organics. J Membrane Sci. 2011; 379(1-2):131–137.
7. Virkutyte J, Varma RS. Green synthesis of metal nanoparticles: Biodegradable polymers and enzymes in stabilization and surface functionalization. Chem Sci. 2011; 2(5):837–846.

8. Zhao DY, He F, Liu JC, Roberts CB. Stabilization of Fe-Pd nanoparticles with sodium carboxymethyl cellulose for enhanced transport and dechlorination of trichloroethylene in soil and groundwater. Ind Eng Chem Res. 2007; 46(1):29–34.
9. Liu JC, He F, Durham E, Zhao DY, Roberts CB. Polysugar-stabilized Pd nanoparticles exhibiting high catalytic activities for hydrodechlorination of environmentally deleterious trichloroethylene. Langmuir. 2008; 24(1):328–336. [PubMed: 18044944]
10. Lowry GV, Phenrat T, Saleh N, Sirk K, Kim HJ, Tilton RD. Stabilization of aqueous nanoscale zerovalent iron dispersions by anionic polyelectrolytes: adsorbed anionic polyelectrolyte layer properties and their effect on aggregation and sedimentation. Journal of Nanoparticle Research. 2008; 10(5):795–814.
11. Tilton RD, Sirk KM, Saleh NB, Phenrat T, Kim HJ, Dufour B, Ok J, Golas PL, Matyjaszewski K, Lowry GV. Effect of Adsorbed Polyelectrolytes on Nanoscale Zero Valent Iron Particle Attachment to Soil Surface Models. Environ Sci Technol. 2009; 43(10):3803–3808. [PubMed: 19544891]
12. Muller RN, Laurent S, Forge D, Port M, Roch A, Robic C, Elst LV. Magnetic iron oxide nanoparticles: Synthesis, stabilization, vectorization, physicochemical characterizations, and biological applications. Chemical Reviews. 2008; 108(6):2064–2110. [PubMed: 18543879]
13. Mirkhalaf F, Paprotny J, Schiffrin DJ. Synthesis of metal nanoparticles stabilized by metal-carbon bonds. J Am Chem Soc. 2006; 128(23):7400–7401. [PubMed: 16756268]
14. Li D, Kaner RB. Shape and aggregation control of nanoparticles: Not shaken, not stirred. J Am Chem Soc. 2006; 128(3):968–975. [PubMed: 16417388]
15. Bhattacharyya D, Xu J. Modeling of Fe/Pd nanoparticle-based functionalized membrane reactor for PCB dechlorination at room temperature. J Phys Chem C. 2008; 112(25):9133–9144.
16. Choi H, Al-Abed SR, Agarwal S, Dionysiou DD. Synthesis of reactive nano-Fe/Pd bimetallic system-impregnated activated carbon for the simultaneous adsorption and dechlorination of PCBs. Chem Mater. 2008; 20(11):3649–3655.
17. Sunkara B, Zhan JJ, He JB, McPherson GL, Piringer G, John VT. Nanoscale Zerovalent Iron Supported on Uniform Carbon Microspheres for the In situ Remediation of Chlorinated Hydrocarbons. Acs Appl Mater Inter. 2010; 2(10):2854–2862.
18. Zahran EM, Bhattacharyya D, Bachas LG. Development of reactive Pd/Fe bimetallic nanotubes for dechlorination reactions. Journal of Materials Chemistry. 2011; 21(28):10454–10462.
19. Benoit R, Warmont F, Meynen V, De Witte K, Cool P, Treguer-Delapierre M, Saboungi ML. Optimisation of the surface properties of SBA-15 mesoporous silica for in-situ nanoparticle synthesis. Microporous and Mesoporous Materials. 2009; 120(1-2):2–6.
20. Lim WTL, Zhong Z, Borgna A. An effective sonication-assisted reduction approach to synthesize highly dispersed Co nanoparticles on SiO_2. Chemical Physics Letters. 2009; 471:122–127.
21. Seger B, Kongkanand A, Vinodgopal K, Kamat PV. Platinum dispersed on silica nanoparticle as electrocatalyst for PEM fuel cell. Journal of Electroanalytical Chemistry. 2008; 621(2):198–204.
22. Wallace JM, Stroud RM, Pietron JJ, Long JW, Rolison DR. The effect of particle size and protein content on nanoparticle-gold-nucleated cytochrome c superstructures encapsulated in silica nanoarchitectures. Journal of Non-Crystalline Solids. 2004; 350:31–38.
23. Zhang SB, Wang JK, Liu HT, Wang XL. One-pot synthesis of Ni-nanoparticle-embedded mesoporous titania/silica catalyst and its application for CO(2)-reforming of methane. Catal Commun. 2008; 9(6):995–1000.
24. Zheng TH, Zhan JJ, He JB, Day C, Lu YF, Mcpherson GL, Piringer G, John VT. Reactivity characteristics of nanoscale zerovalent iron-silica composites for trichloroethylene remediation. Environmental Science & Technology. 2008; 42(12):4494–4499. [PubMed: 18605576]
25. Zhan JJ, Zheng TH, Piringer G, Day C, McPherson GL, Lu YF, Papadopoulos K, John VT. Transport Characteristics of Nanoscale Functional Zerovalent Iron/Silica Composites for in Situ Remediation of Trichloroethylene. Environmental Science & Technology. 2008; 42(23):8871–8876. [PubMed: 19192811]
26. a Impens NREN, van der Voort P, Vansant EF. Silylation of micro-, meso- and non-porous oxides: a review. Microporous and Mesoporous Materials. 1999; 28(2):217–232.b Ariga K, Vinu A,

Hossain KZ. Recent advances in functionalization of mesoporous silica. Journal of Nanoscience and Nanotechnology. 2005; 5(3):347–371. [PubMed: 15913241]

27. Meeks ND, Rankin S, Bhattacharyya D. Sulfur-Functionalization of Porous Silica Particles and Application to Mercury Vapor Sorption. Ind Eng Chem Res. 2010; 49(10):4687–4693.
28. Meyer DE, Meeks N, Sikdar S, Hutson ND, Hua D, Bhattacharyya D. Copper-doped silica materials silanized with bis-(triethoxy silyl propyl)-tetra sulfide for mercury vapor capture. Energ Fuel. 2008; 22(4):2290–2298.
29. Miyake Y, Sakoda A, Yamanashi H, Kaneda H, Suzuki M. Activated carbon adsorption of trichloroethylene (TCE) vapor stripped from TCE-contaminated water. Water Res. 2003; 37(8): 1852–1858. [PubMed: 12697228]
30. Serrano DP, Calleja G, Sanz R, Pizarro P. Development of crystallinity and photocatalytic properties in porous TiO2 by mild acid treatment. Journal of Materials Chemistry. 2007; 17(12): 1178–1187.
31. De Laat J, Gallard H. Catalytic decomposition of hydrogen peroxide by Fe(III) in homogeneous aqueous solution: Mechanism and kinetic modeling. Environ Sci Technol. 1999; 33(16):2726–2732.
32. Lewis S, Lynch A, Bachas L, Hampson S, Ormsbee L, Bhattacharyya D. Chelate-Modified Fenton Reaction for the Degradation of Trichloroethylene in Aqueous and Two-Phase Systems. Environ Eng Sci. 2009; 26(4):849–859. [PubMed: 20418966]
33. Xu J, Bhattacharyya D. Membrane-based bimetallic nanoparticles for environmental remediation: Synthesis and reactive properties. Environmental Progress. 2005; 24(4):358–366.
34. Jin S, Fallgren PH, Morris JM, Edgar ES. Degradation of trichloroethene in water by electron supplementation. Chem Eng J. 2008; 140(1-3):642–645.
35. Tee YH, Grulke E, Bhattacharyya D. Role of Ni/Fe nanoparticle composition on the degradation of trichloroethylene from water. Ind Eng Chem Res. 2005; 44(18):7062–7070.
36. Zhao DY, He F. Hydrodechlorination of trichloroethene using stabilized Fe-Pd nanoparticles: Reaction mechanism and effects of stabilizers, catalysts and reaction conditions. Applied Catalysis B-Environmental. 2008; 84(3-4):533–540.
37. Liu HL, Wang XY, Chen C, Ma J. Characterization and Evaluation of Catalytic Dechlorination Activity of Pd/Fe Bimetallic Nanoparticles. Ind Eng Chem Res. 2008; 47(22):8645–8651.
38. Iler, RK. The Chemistry of Silica. Wiley; New York: 1979.
39. Christy AA, Egeberg PK. Quantitative determination of surface silanol groups in silicagel by deuterium exchange combined with infrared spectroscopy and chemometrics. Analyst. 2005; 130(5):738–744. [PubMed: 15852145]
40. Bukur DB, Lang XS. Highly active and stable iron Fischer-Tropsch catalyst for synthesis gas conversion to liquid fuels. Industrial & Engineering Chemistry Research. 1999; 38(9):3270–3275.
41. Nath M, Satishkumar BC, Govindaraj A, Vinod CP, Rao CNR. Production of bundles of aligned carbon and carbon-nitrogen nanotubes by the pyrolysis of precursors on silica-supported iron and cobalt catalysts. Chem Phys Lett. 2000; 322(5):333–340.
42. a Bukur DB, Lang X, Mukesh D, Zimmerman WH, Rosynek MP, Li CP. Binder Support Effects on the Activity and Selectivity of Iron Catalysts in the Fischer-Tropsch Synthesis. Industrial & Engineering Chemistry Research. 1990; 29(8):1588–1599.b Jin YM, Datye AK. Phase transformations in iron Fischer-Tropsch catalysts during temperature-programmed reduction. J Catal. 2000; 196(1):8–17.
43. Wielers AFH, Kock AJHM, Hop CECA, Geus JW, Vanderkraan AM. The Reduction Behavior of Silica-Supported and Alumina-Supported Iron Catalysts - a Mossbauer and Infrared Spectroscopic Study. J Catal. 1989; 117(1):1–18.
44. Varma RS, Hoag GE, Collins JB, Holcomb JL, Hoag JR, Nadagouda MN. Degradation of bromothymol blue by ‘greener’ nano-scale zero-valent iron synthesized using tea polyphenols. J Mater Chem. 2009; 19(45):8671–8677.
45. Liu JC, He F, Gunn TM, Zhao DY, Roberts CB. Precise Seed-Mediated Growth and Size-Controlled Synthesis of Palladium Nanoparticles Using a Green Chemistry Approach. Langmuir. 2009; 25(12):7116–7128. [PubMed: 19309120]

46. De Corte S, Hennebel T, Fitts JP, Sabbe T, Bliznuk V, Verschuere S, Van der Lelie D, Verstraete W, Boon N. Biosupported bimetallic Pd--Au nanocrystals for dechlorination of environmental contaminants. Environ Sci Technol. 2011

47. a Varma RS, Nadagouda MN. Green synthesis of Ag and Pd nanospheres, nanowires, and nanorods using vitamin B(2): Catalytic polymerisation of aniline and pyrrole. J Nanomater. 2008b Varma RS, Nadagouda MN, Polshettiwar V. Self-assembly of palladium nanoparticles: synthesis of nanobelts, nanoplates and nanotrees using vitamin B(1), and their application in carbon-carbon coupling reactions. J Mater Chem. 2009; 19(14):2026–2031.

48. a Kitajima N, Fukuzumi S, Ono Y. Formation of Superoxide Ion during Decomposition of Hydrogen-Peroxide on Supported Metal-Oxides. Journal of Physical Chemistry. 1978; 82(13): 1505–1509.b Lin SS, Gurol MD. Catalytic decomposition of hydrogen peroxide on iron oxide: Kinetics, mechanism, and implications. Environmental Science & Technology. 1998; 32(10): 1417–1423.

49. Yeh CK-J, Chen W-S, Chen W-Y. Production of hydroxyl radicals from the decomposition of hydrogen peroxide catalyzed by various iron oxides at pH 7. Practice Periodical of Hazardous, Toxic, and Radioactive Waste Management. 2004; 8(3)

50. Miller CM, Valentine RL. Hydrogen-Peroxide Decomposition and Quinoline Degradation in the Presence of Aquifer Material. Water Res. 1995; 29(10):2353–2359.

51. Watts RJ, Jones AP, Chen PH, Kenny A. Mineral-catalyzed Fenton-like oxidation of sorbed chlorobenzenes. Water Environment Research. 1997; 69(3):269–275.

52. Doyle FM, Pham ALT, Lee C, Sedlak DL. A Silica-Supported Iron Oxide Catalyst Capable of Activating Hydrogen Peroxide at Neutral pH Values. Environ Sci Technol. 2009; 43(23):8930–8935. [PubMed: 19943668]

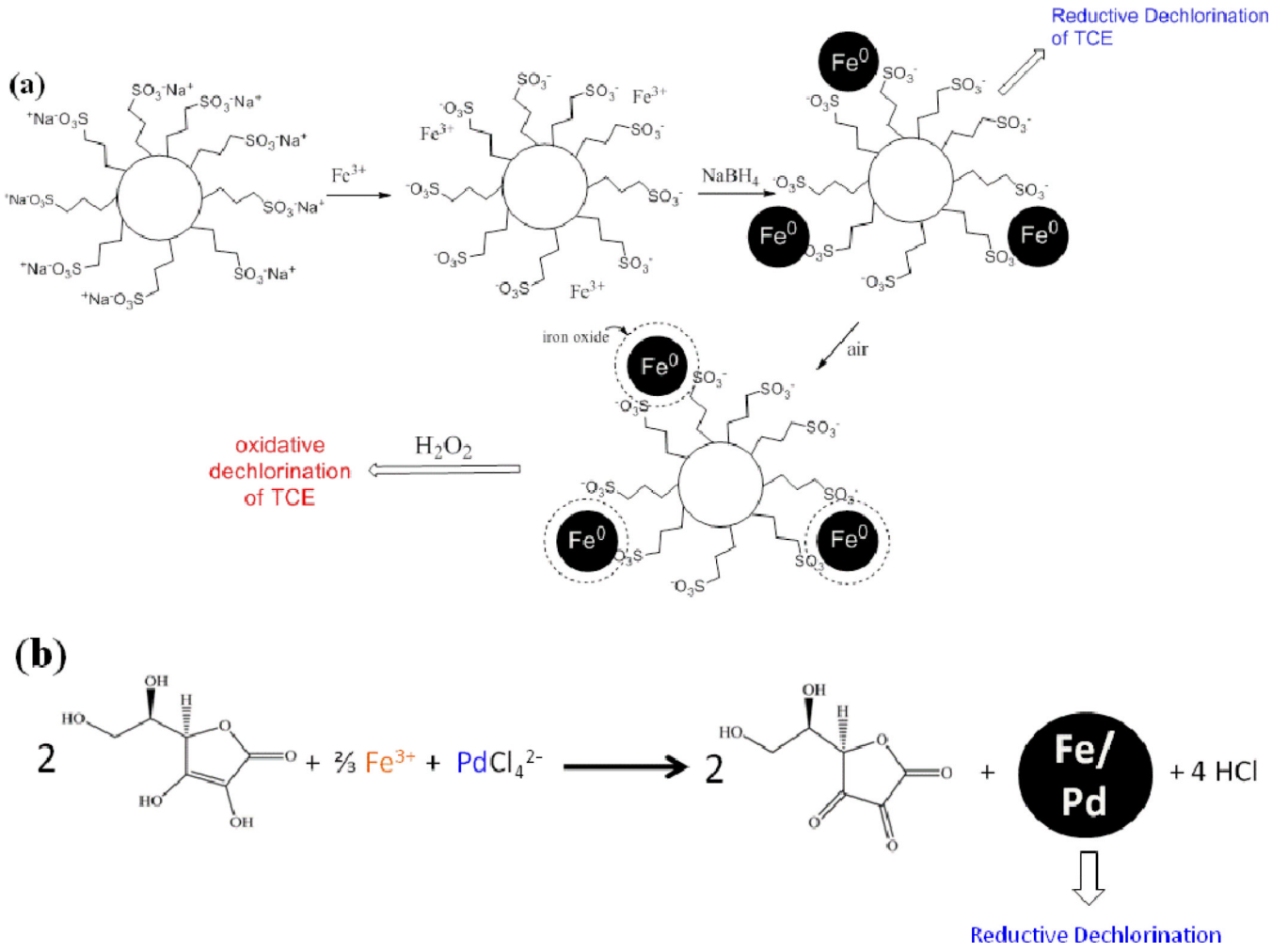

Figure 1.

Schematic of various Fe and Fe/Pd nanoparticle synthesis. (a) Silica-gel based synthesis of zero-valent iron nanoparticles for reductive dechlorination or iron/iron oxide nanoparticles for oxidative dechlorination. (b) “green” synthesis of bimetallic particles where excess reducing agent inhibits oxidation as well as agglomeration of particles. In this reaction, ascorbic acid is oxidized to dehydroascorbic acid.

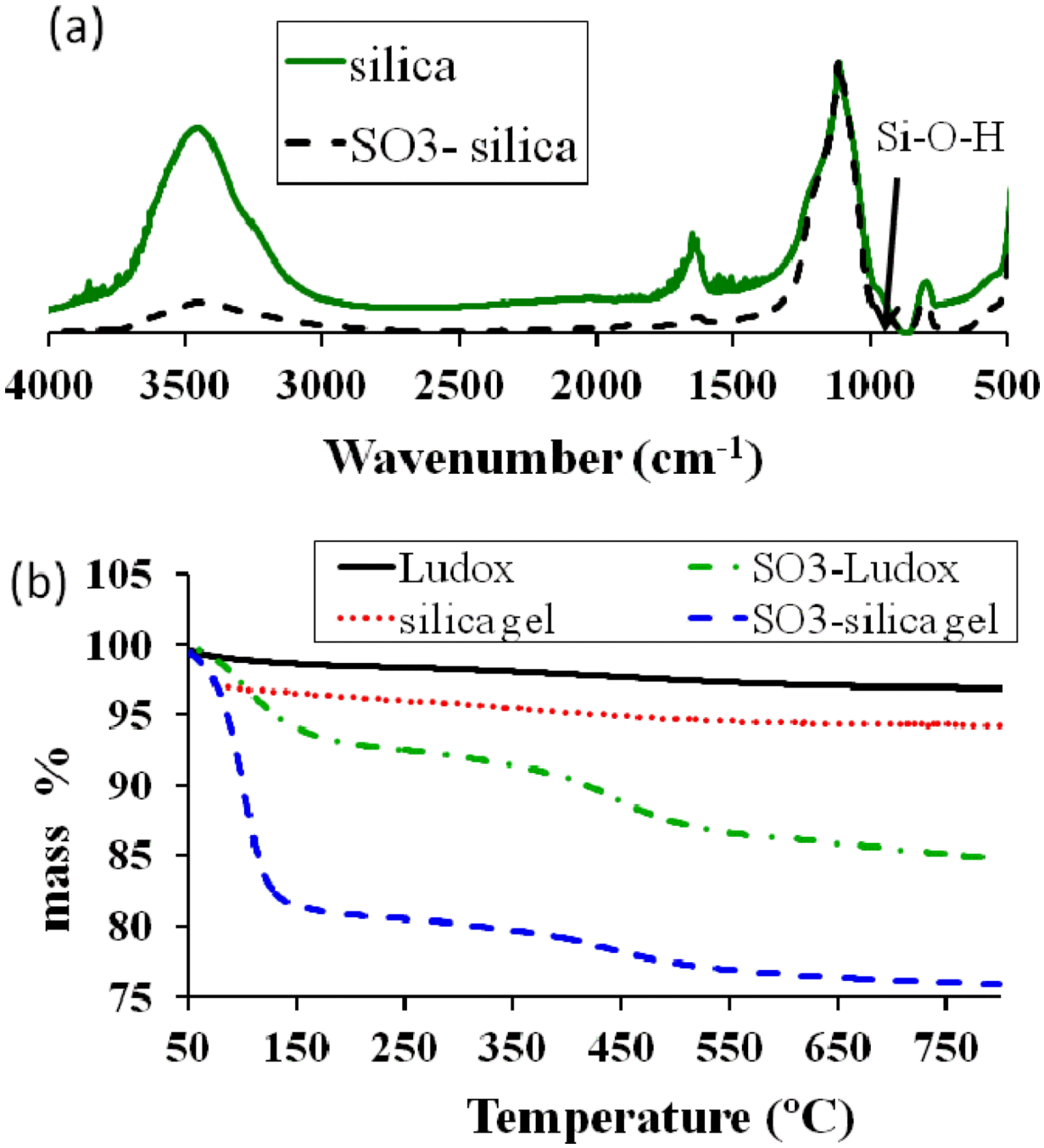

Figure 2.

Two methods for measuring extent of silica functionalization are normalized FT-IR spectra and thermogravimetric analysis. Heating rate: 10 °C/min. (a) Representative normalized FT-IR spectra for sulfonate-functionalized Ludox silica and unfunctionalized silica. The peak at 980 cm^{-1} indicates the surface Si-OH, which decreases upon functionalization. (b) Representative TGA for sulfonated silica samples.

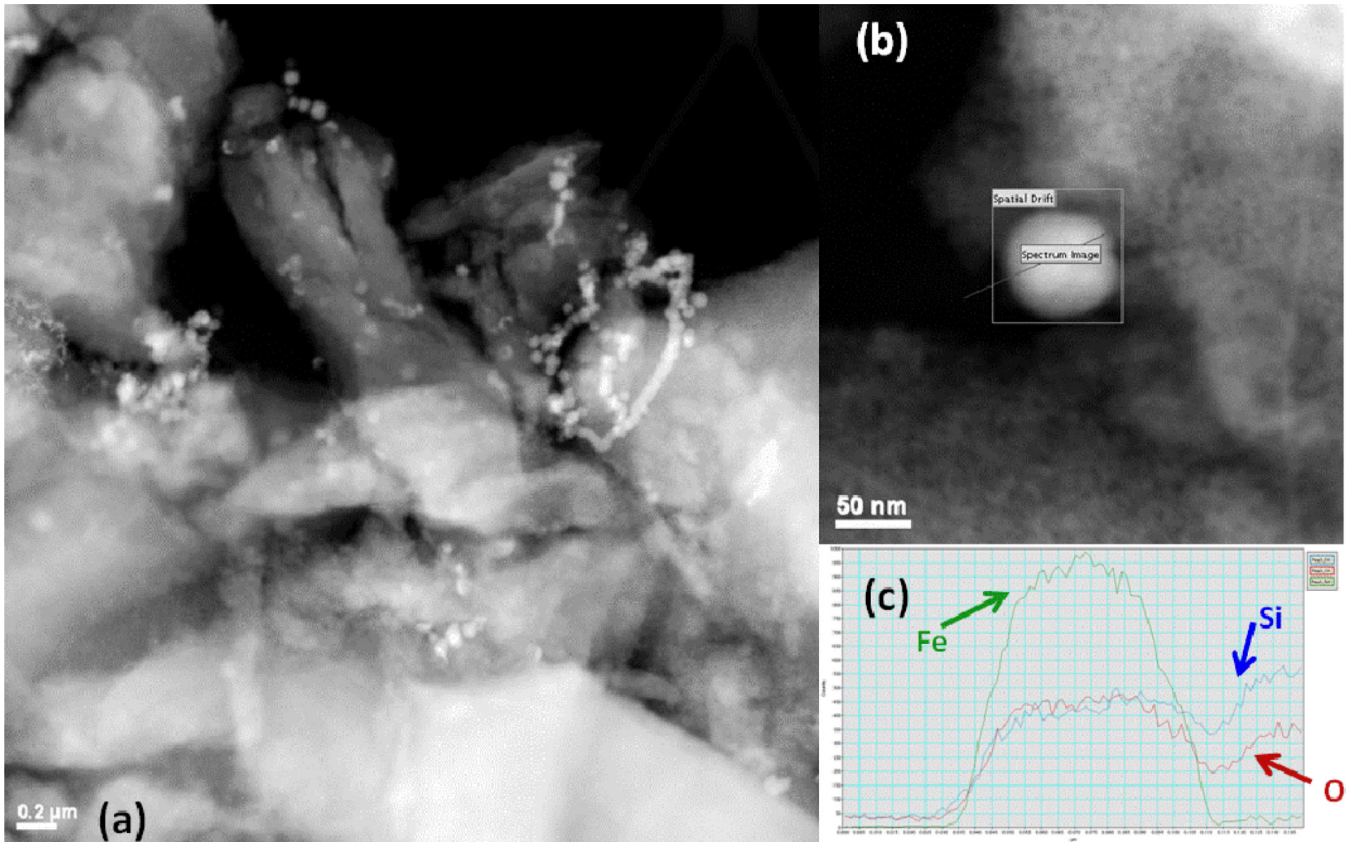

Figure 3.
Transmission electron micrographs of Fe particles on silica gel. (a) Fe particles (~50 nm) formed on surface and in the pores of silica gel. Brighter spots indicate Fe (higher atomic number). Scale bar is 200 nm. (b) Higher resolution image of spherical Fe nanoparticles with path indicating line scan for EDS. (c) EDS confirms elemental Fe composition of particle with silica background.

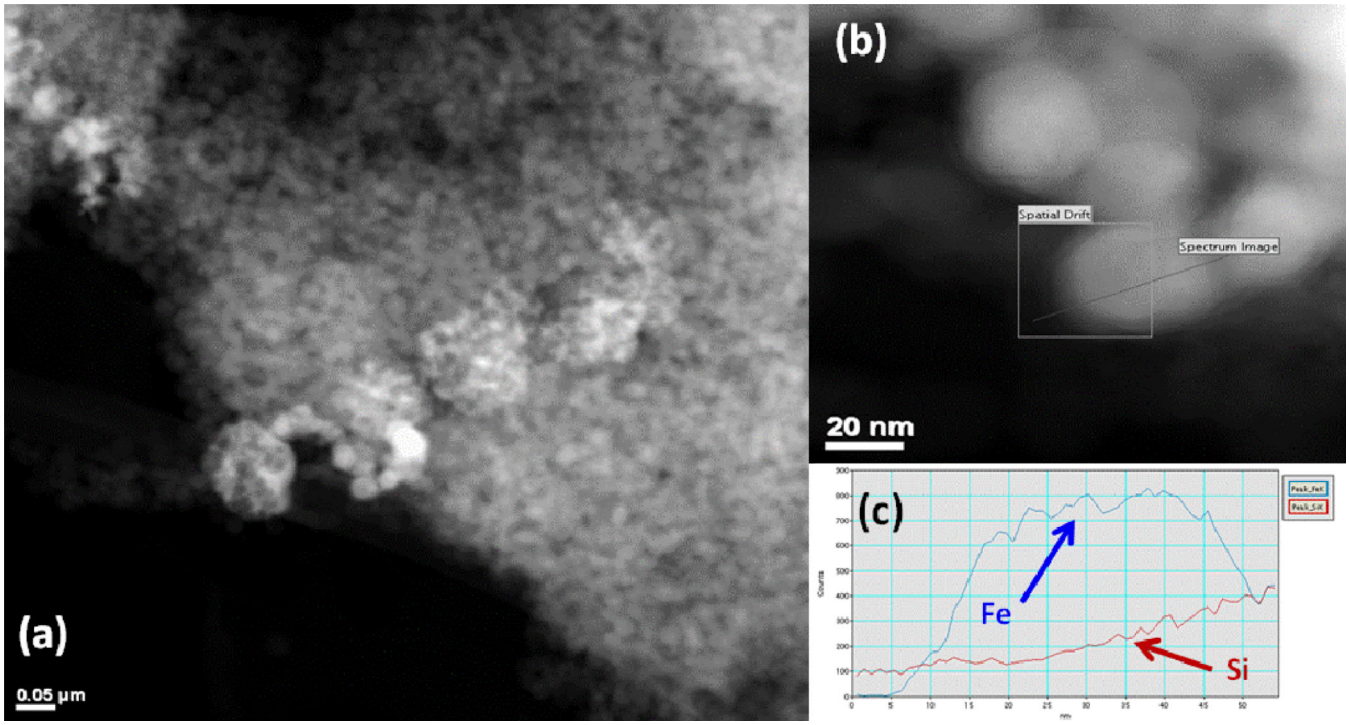

Figure 4.

Transmission electron micrographs of Fe particles on Ludox silica. (a) Fe particles (30-50 nm) formed on surface of silica nanoparticles (22 nm). Brighter spots indicate Fe (higher atomic number). Scale bar is 50 nm. (b) Higher resolution image of spherical Fe nanoparticles with path indicating line scan for EDS. (c) EDS confirms elemental Fe composition of particle with silica background.

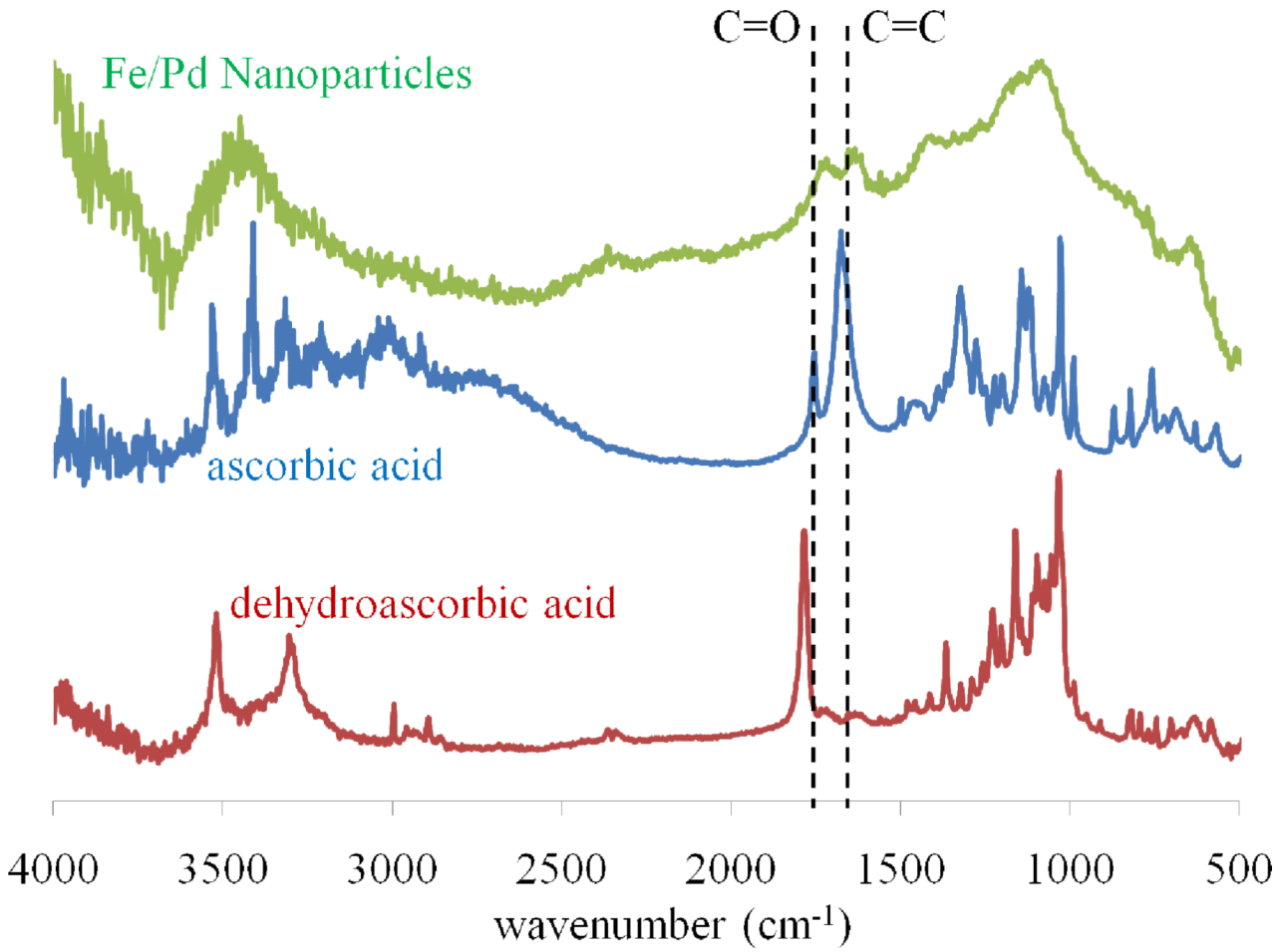

Figure 5.
IR spectra of known ascorbic acid and dehydroascorbic acid (structures shown in Figure 1) with Fe/Pd nanoparticles synthesized by reduction with ascorbic acid. The nanoparticle spectrum indicates both ascorbate ion (C=C bond) and dehydroascorbic acid (C=O bond) adsorb to the nanoparticle surface. (Ascorbate ion is present above pH 4.7)

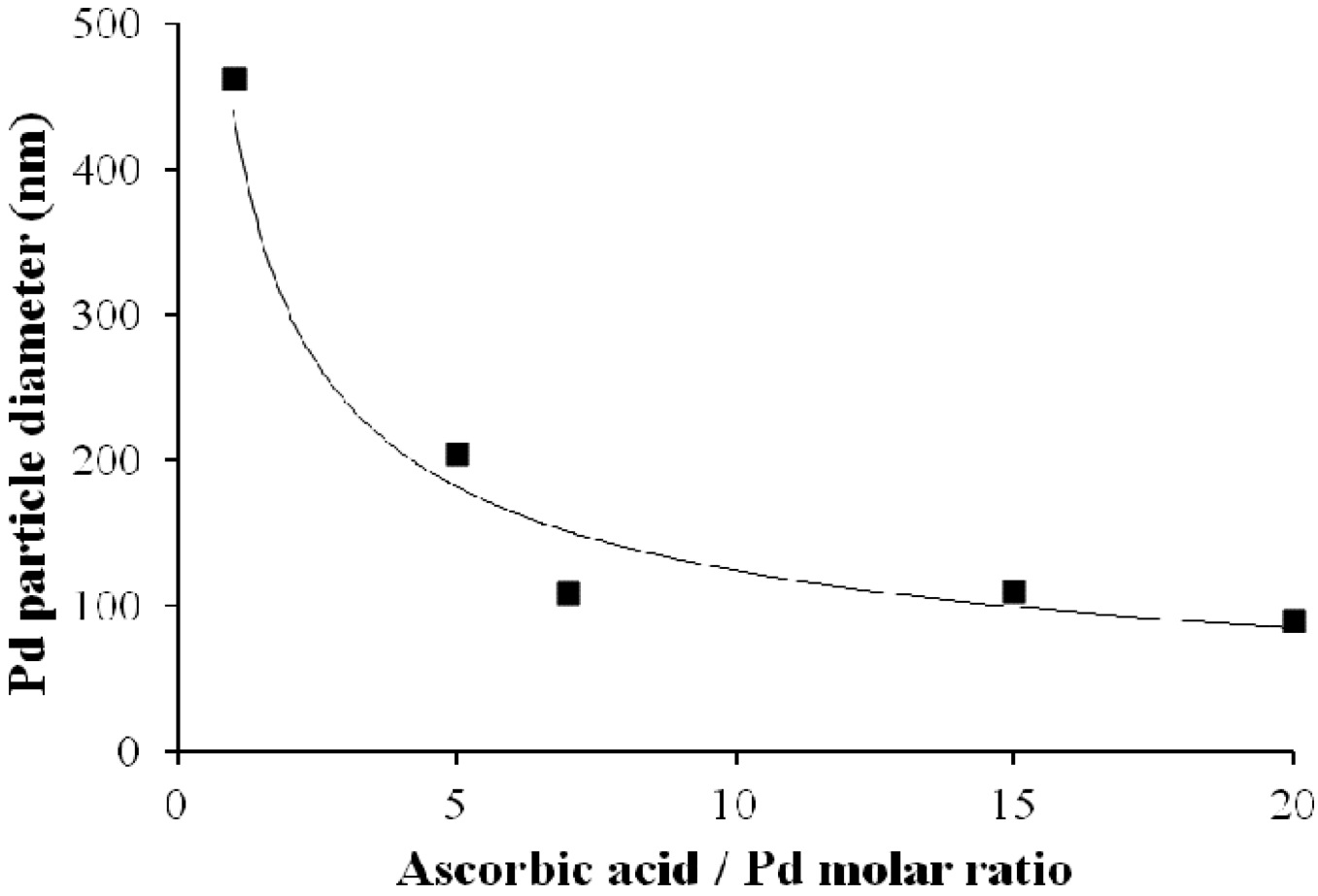

Figure 6.
Decrease in particle size (hydrodynamic radius measured by DLS) for Pd particles synthesized by reduction with ascorbic acid, due to presence of surface adsorption of excess ascorbate and dehydroascorbic acid. The synthesis reaction is same as presented in Figure 1, without the presence of Fe.

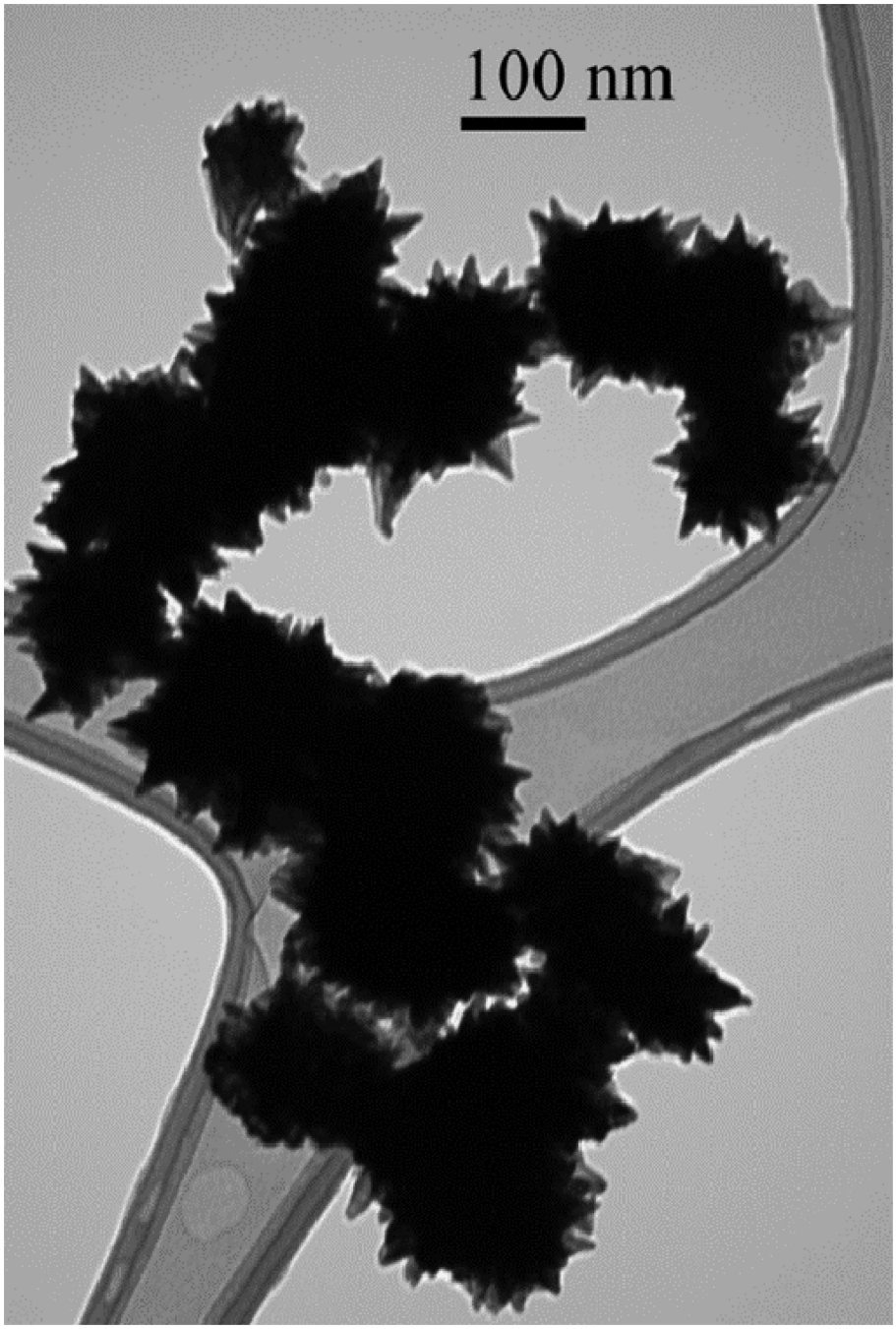

Figure 7.
TEM of ascorbic acid-synthesized Fe/Pd NP at lower pH (<4.2).

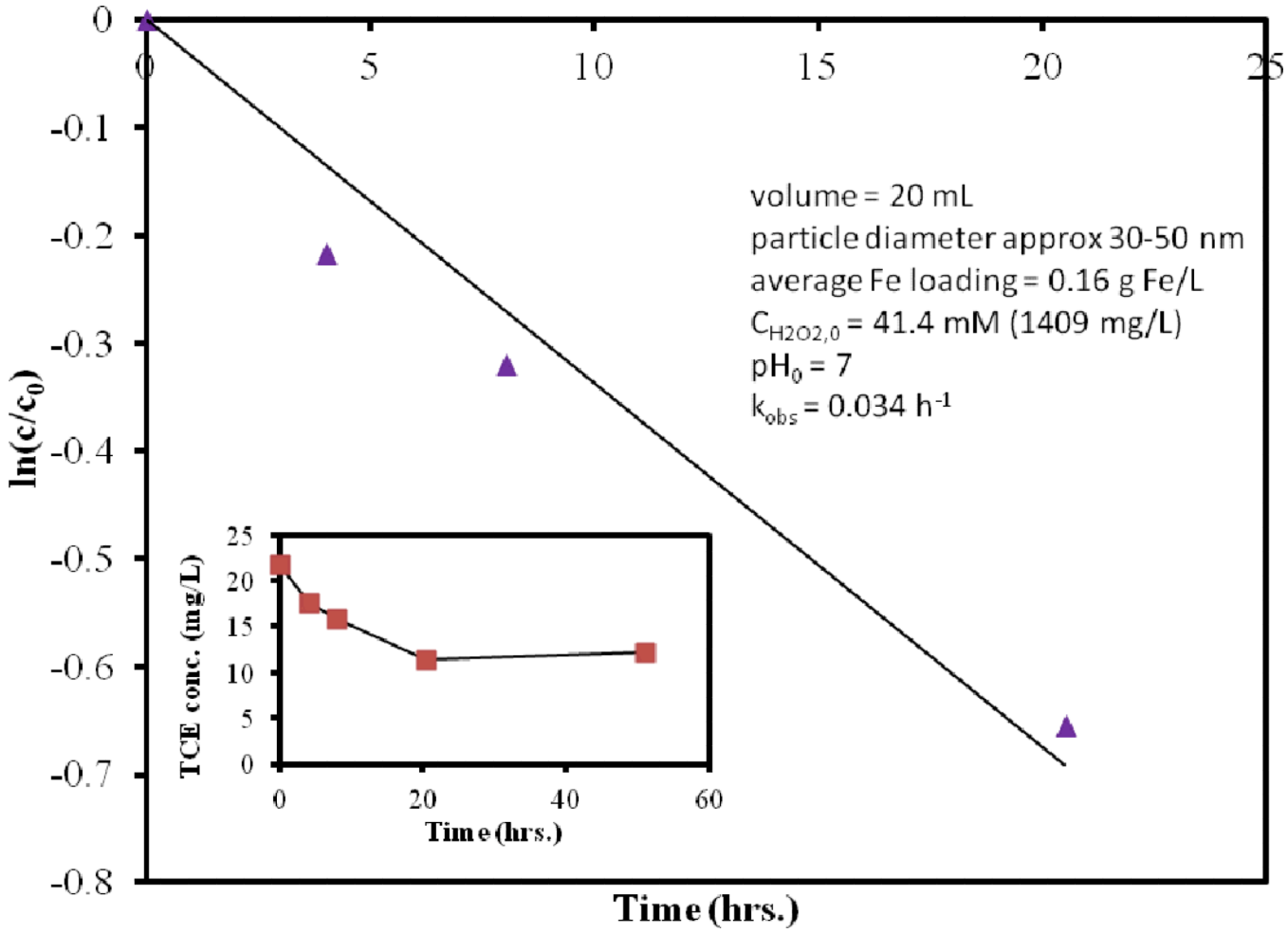

Figure 8.
Oxidative degradation of trichloroethylene by air-oxidized Fe/Fe_2O_3 particles on Ludox by hydroxyl radical reaction (use of H_2O_2). $C_{TCE,0}$ = 21.5 mg/L.

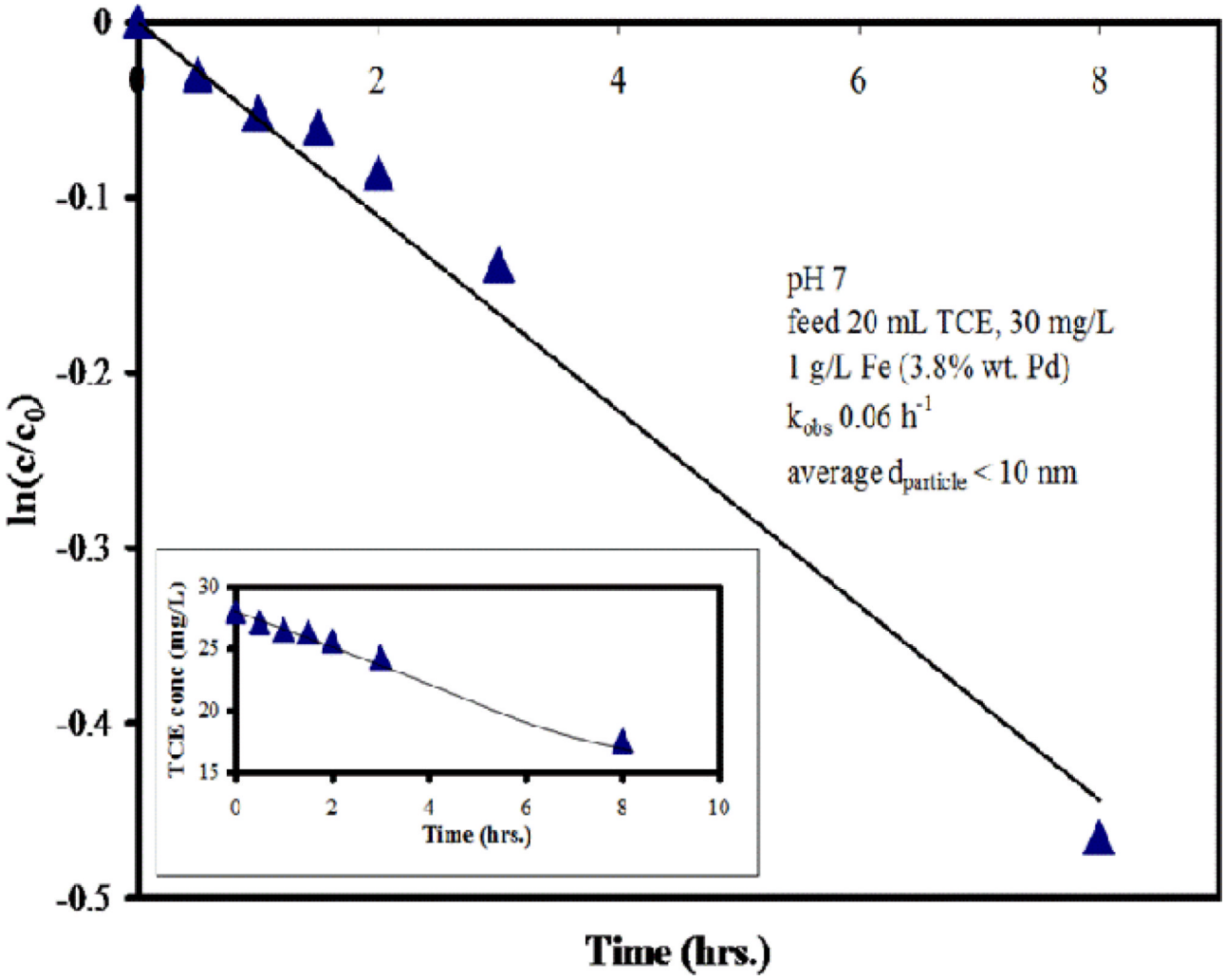

Figure 9.
Reductive degradation of trichloroethylene by Fe/Pd particles synthesized by reduction with ascorbic acid. $C_{TCE,0}$ = 27 mg/L

Table 1

Structural characteristics of unfunctionalized and functionalized silica samples used as platform for nanoparticle synthesis.

		BET surface area (m^2/g):		
	Aggregate size (μm)	**before functionalization**	**After functionalization**	**Fe NP-silica**
Ludox	0.022	87	92	110
Silica gel	3.7	585	264	224

Table 2

Reactions for the “green” synthesis of Fe/Pd bimetallic nanoparticles by ascorbic acid. (see Figure 1 for chemical structures)

Reaction	E^0 value (V)
2 Ascorbic acid $\rightarrow$ 2 dehydroascorbic acid + 4 e^- + $4H^+$	-0.116
2/3 Fe^{3+} + 2e^- $\rightarrow$ 2/3 Fe^0	-0.0247
Pd^{2+} + 2e^- $\rightarrow$ Pd^0	+0.951
Overall:	
2 Ascorbic acid + 2/3 Fe^{3+} + Pd^{2+} $\rightarrow$ 2 dehydroascorbic acid + 2/3 Fe^0 + Pd^0 + $4H^+$	+0.810V